# ANALITYCAL DESCRIPTION OF THE NON-LINEAR RESPONSE OF CRESCENT SHAPED BRACES HYSTERETIC DEVICES

G. Gasparini[(1)], M. Palermo[(2)], V. Laghi[(3)], S. Silvestri[(4)], T. Trombetti[(5)]

[(1)] *Associate professor, Department of Civil, Chemical, Environmental and Materials Engineering, University of Bologna, giada.gasparini4@unibo.it*

[(2)] *Assistant professor, Department of Civil, Chemical, Environmental and Materials Engineering, University of Bologna, michele.palermo7@unibo.it*

[(3)] *Ph.D candidate, Department of Civil, Chemical, Environmental and Materials Engineering, University of Bologna, vittoria.laghi2@unibo.it*

[(4)] *Associate professor, Department of Civil, Chemical, Environmental and Materials Engineering, University of Bologna, stefano.silvestri@unibo.it*

[(5)] *Associate professor, Department of Civil, Chemical, Environmental and Materials Engineering, University of Bologna, tomaso.trombetti@unibo.it*

## *Abstract*

The present work investigates the non-linear behavior of a steel hysteretic dissipative device known in the literature as Crescent Shaped Braces. The interaction between non-linear material behavior and non-linear geometrical effects due to the peculiar device shape results in a complex non-linear force-displacement response that can be controlled varying the key geometrical parameters. In this way the device can be efficiently utilized as a dissipative bracing capable of satisfying multiple seismic design objectives within a seismic design approach based on multiple building performances. In this work, simplified analytical relationships able to describe the key features of the device non-linear behavior are derived. Their effectiveness is then verified by mean of numerical simulations.

*Keywords: Crescent Shaped Braces; non-linear behavior; analytical description, numerical simulations, performance based seismic design.*

## 1. Introduction

Traditional seismic design code procedures up to the end of 1990s were grounded on force-based approaches with the specific aim of providing the required strength capacities against a single limit state (typically a ultimate limit state), and then verifying the whole performances against the other limit states. Nevertheless, the high severe damages caused by major earthquakes in the 1990s such as the 1994 Northridge Earthquake which was one of the most costly earthquake in U.S. history, or the 1995 Kobe earthquake, revealed the need of a new design approach aimed at controlling the structural response under various seismic intensity levels thus avoiding excessive damages.

A change of paradigm has been postulated after those dramatic earthquakes with the conceptual framework of Performance Based Seismic Design (PBSD) first proposed by SEAOC (1995) [1]. PBSD framework theoretically encompasses the full range of seismic engineering issues toward predictable and controlled seismic performances under established multiple earthquake intensity levels [2,3]. PBSD procedures could permit to actively control the whole response of the structure under different input intensity levels.

One possibility to exploit the PBSD approach at best is based on the use of specific dissipation devices such as steel dampers. In the past decades several solutions have been proposed including: U-shaped dampers, buckling restrained braces (BRB), steel plate-based dampers (such as ADAS, TADAS, X-shaped dampers, comb-teeth, curved steel dampers), steel shear panel-based dampers, J-dampers, pipe-based dampers [4-15]. The work by Javanmardi et al. [16] provides a state-of-the art review of metallic dampers.

Among the proposed solutions, a hysteretic steel brace, called Crescent Shaped Braces (CSB), has been investigated by the authors since 2009 [17]. CSBs are characterized by a peculiar geometrical shape resulting in a non-symmetric force-displacement response whose main features (stiffness $k_{in}$, first yield strength $F_y$, ductility $\mu$, ultimate strength $F_u$) can be ad-hoc designed based on the imposition of different performance objectives (POs) [18–20]. The mechanical behavior of the single CSB has already been widely investigated in the past by means of analytical, numerical and experimental investigations [18,21]. In these studies the attention was mainly devoted to the behavior in tension from which analytical expressions for the initial stiffness kin and first yielding force $F_y$ were derived. The present work provides further insights into the non-linear force-displacement behavior of the CSB device. First, general considerations on the relationship between the CSB geometrical properties and non-linear geometrical effects and their influence upon the force-displacement behavior are provided. Then, analytical relationships of the mechanical behavior parameters governing the whole non-linear behavior of the CSB are derived. Also, direct design formulations useful for the preliminary design are proposed.

## 2. The Crescent Shaped Brace device

The Crescent Shaped Brace (CSB) is a steel hysteretic device connecting two points of the structure through an element with a curved (or also bi-linear) shape leading to the coupling of flexural and axial behavior. When inserted into a frame (Figure 1), the CSB acts as a yielding brace with a highly non-linear force-displacement response [19]. In particular, Figure 1 qualitatively depicts the cyclic lateral force vs lateral displacement (F-u) response of both (i) a single CSB as inserted into a single-bay frame and (ii) a couple of CSBs as inserted into two adjacent bays of a frame, so that while one device works in tension, the other one works in compression (and vice-versa). From a general point of view, the cyclic lateral force-displacement response of the single CSB is strongly asymmetric in tension and compression. On the contrary, the whole F-u behavior of the couple of CSBs is symmetric since the two devices work in parallel.

The strong asymmetry in the response of the single CSB is due to the coupling of mechanical and geometrical non-linear effects leading to: (i) a significant hardening after first yielding of the knee point when the brace is subjected to tension (the red backbone curve of Figure 1a), the hardening being mainly due to the progressive reduction of the lever arm; (ii) a smooth softening in compression, after the peak capacity is achieved (the green backbone curve of Figure 1a).
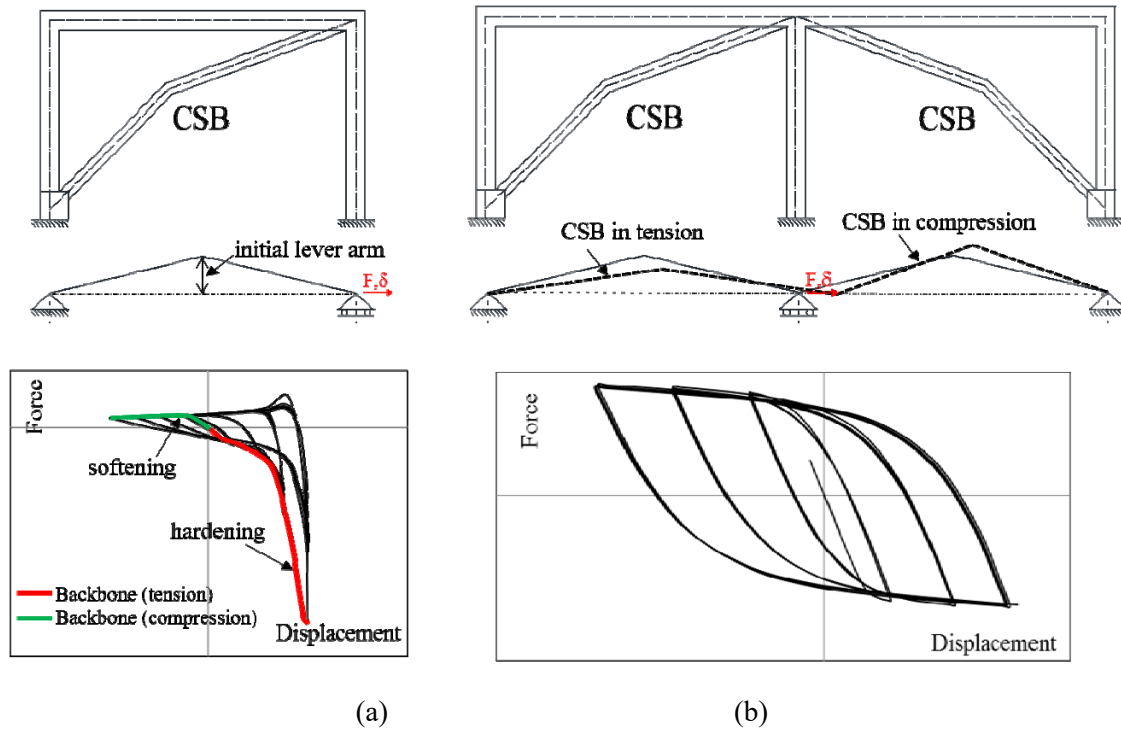
Figure 1 - Cyclic force-displacement behavior: (a) single CSB inserted in a single-bay frame; (b) couple of CSBs inserted into two adjacent bays of a frame. (adapted from [21]).

This complex F-u behavior and the possibility of calibrating the geometrical parameters to obtain different responses make the CSB suitable as the base component of a lateral resisting system capable of achieving different performance objectives within the Performance-Based Seismic Design framework [17].

The design steps from the selection of the POs to the sizing of each CSB are conceptually depicted in the flow chart reported in Figure 2. First, target values of the mechanical behavior objectives for the whole lateral resisting system, namely the initial stiffness $\overline{k_{in}}$, the yielding force $\overline{F_y}$ and the displacement ductility capacity $\overline{\mu}$ for the entire lateral-resisting system (LRS) are evaluated. The next step is to obtain the target values of the mechanical behavior objectives for each CSB (namely $\overline{k_{in,CSB}}$, $\overline{F_{y,CSB}}$, $\overline{\mu_{CSB}}$). The final step deals with the sizing of the main geometrical properties which govern the design of each device.
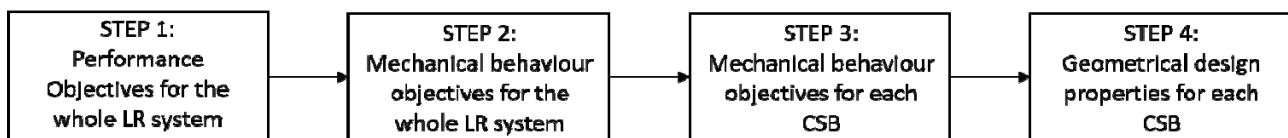


Figure 2 - Design steps from the identification of the PO to the sizing of each CSB device.

## 2.1 Geometric properties of the "symmetric bilinear CSB" and influence of non-linear geometrical effects on the force-displacement response

3

With the purpose of deriving analytical relationships useful in the preliminary design phase, henceforth the attention will be devoted to the specific CSB configuration made by two straight elements (AC and CB) of equal lengths $L^*$, referred to as "symmetric bilinear CSB" (Figure 3). The angle $\theta_0$ indicates the initial inclination of each straight segment with respect to the horizontal direction. Point A is fixed, while point B is free to move along the lateral direction (u indicates the horizontal displacement). The two end supports do not provide any rotational restraint. One of the main geometrical characteristic of the brace is the "initial lever arm" $d_0$, namely the vertical distance between the axis connecting A to B (whose length is referred to as $2L_0$) and point C. The arm $d_0$ when normalized with respect to the length $2L_0$ is referred to as $\xi_0 = d_0/2L_0$.
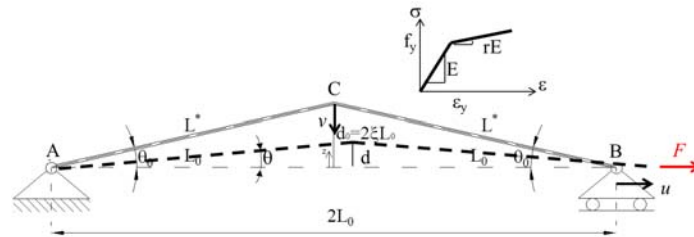


Figure 3 - The "bilinear symmetric" configuration of a CSB subjected to a lateral force F (adapted from [21]).

For the sake of clearness, the geometrical and material properties of a "symmetric bilinear CSB" are reported below:

*Global geometrical properties:*
- $L^*$: length of each straight element.
- $L_0$: projection of L* in the horizontal plane.
- $\xi_0 = d_0 / 2L_0$ =normalized initial lever arm.

*Cross section properties:*
- $h$= cross-sectional height.
- $A$=cross-sectional area of each straight element.
- $J$=cross-sectional moment of inertia (in-plane).
- $i$=radius of gyration ($i = \sqrt{J/A}$).
- $W_e$= elastic strength modulus.
- $\beta$ = plastic benefit ($W_{pl} = \beta \cdot W_{pl}$ is the plastic strength modulus).

*Material properties:*
- $E$= elastic modulus.
- $f_y$ and $\varepsilon_y$= yielding strength and strain.
- $f_u$ and $\varepsilon_u$= ultimate strength and strain.
- $r$= hardening ratio.

When subjected to a lateral force F, the two straight elements of the CSB deform due to the interaction of axial force (compression or tension depending on the direction of F) and bending moment. The angle between the horizontal direction and the chord of one CSB segment in the generic deformed configuration is indicated with $\theta$ and the corresponding arm is indicated with $d$. The vertical displacement of point C is indicated with $v$.

4

The axial force and bending moment initially depend on the value of $d_0$: the larger $d_0$, the higher the bending moment with respect to the axial force (and vice versa). Similarly, their variations depend on the variation of the lever arm d and influence the CSB force-displacement behavior. As anticipated in the previous section, the lateral force-displacement response of a CSB is governed by both non-linear mechanical and geometrical effects. Non-linear mechanical behavior is related to material stress-strain behavior. Non-linear geometrical effects are depending on the variation of the geometrical configuration, mainly depending on the evolution of the arm *d*. As such, at first approximation, an initial appraisal of the second-order effects on the force-displacement curve can be carried out by analyzing the kinematic behavior of the equivalent rigid system, e.g. a system made of two rigid straight segments having the same global geometry of the CSB and supposed to be pinned in C. The kinematic behavior of such system is described by one unique degree of freedom, for instance the angle $\theta$ that relates the two displacement components *u* and *v*:

$$u = 2L^* \left( \cos\theta - \cos\theta_0 \right)$$
$$v = L^* \left( \sin\theta_0 - \sin\theta \right)$$ 

(1)

From simple trigonometric relationships, the incremental displacements dv and du are related by:

$$\frac{dv}{du} = \frac{1}{2}\tan^{-1}\theta$$ 

(2)

Figure 4 displays the trend of $\dfrac{dv}{du}$ with respect to the normalized arm $\xi$. It is clear that second order effects cannot be ignored when the incremental displacement dv become much larger than the corresponding incremental displacement du, this happen when $\dfrac{dv}{du} \gg 1.0$ .
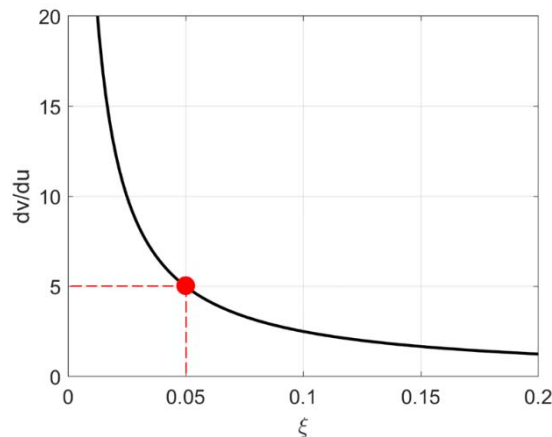


Figure 4 - $\dfrac{dv}{du}$ vs $\xi$.

For practical purposes, a value of $\dfrac{dv}{du} = 5$ can be assumed as a reference value. From Figure 4, it can be noted that the condition $\dfrac{dv}{du} = 5$ occurs for a normalized arm equal to 5%. From this evidence, it follows that a CSB device with an initial lever arm $\xi < 5\%$ will be characterized by a F-u behavior significantly influenced by non-linear geometrical effects from relatively small values of lateral displacement (premature hardening), therefore with limited ductile capacity. On the contrary, for CSBs with larger initial lever arm, the non-linear

5

geometrical effects will be engaged at larger values of lateral displacements, thus allowing the development of a significant ductile behaviour.

The qualitative graphical representations of the F-u curves (or backbone curves) of a single CSB are shown in Figures 5a and b for positive (tension) and negative (compression) values of applied force F, respectively. Figure 5c provides the qualitative representation of the whole F-u curve for a couple of CSBs working in parallel (one CSB works in tension while the other works in compression, and vice-versa).



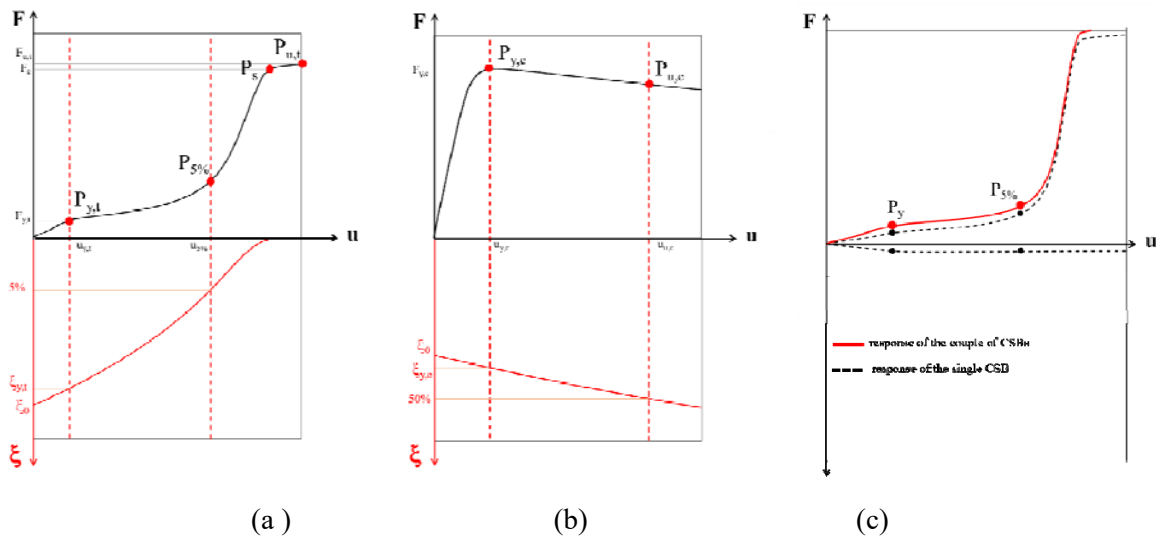(a )                                    (b)                                    (c)

Figure 5 - (a) Backbone curve in tension of the single CSB; (b) Backbone curve in compression of the single CSB. (c) Backbone curve for coupled CSBs.

First the attention is focused on Figure 5a, providing the F-u curve in the upper part of the graph (black curve) and the variation of the normalized arm with the displacement ($\xi$-u curve) in the lower part of the graph (red curve). The tension force-displacement response is made by a first elastic range (governed mainly by the flexural stiffness) until yielding of the knee cross section C. The first yielding point in tension is referred to as $P_{y,t}$. Then, a flexural plastic phase with progressive increase in stiffness due to interaction of non-linear mechanical (material hardening) and geometrical (reduction of the arm $d$) effects is observed. Non-linear geometrical effects do not produce a significant hardening up to point $P_{5\%}$ corresponding to a reduction of normalized arm $\xi$ up to a value equal to 5%. When non-linear geometrical effects become significant a sudden increase in the lateral stiffness occurs due to predominant axial stiffness until the brace reaches the straight configuration (e.g. the arm reduces to zero, $\xi$ =0). This point is referred to as $P_s$. Failure in tension occurs at point $P_u$.

The behavior under lateral forces inducing axial compression and bending moment (Figure 5b) is instead characterized by an initial elastic behavior until the first yielding at the knee point C is achieved (point $P_{y,c}$), then followed by a softening behavior resulting from the interaction of non-linear mechanical (material plastic behaviour) and geometrical (increase in the arm $d$) effects, qualitatively similar to the in-plane buckling behavior of a column with an initial crookedness subjected to an axial force [22]. The coupled response of two CSBs (Figure 5c) is given by the sum of the force carried by each single brace (since they work in parallel). In general, but especially for large displacements, the response is governed by the CSB in tension.

To sum up, the force-displacement response of the CSB can be synthetically described by the following key mechanical properties:
- initial stiffness $k_{in}$;
- first yielding point in tension ($F_{y,t}$, $u_{y,t}$) and compression capacity ($F_{y,c}$, $u_{y,c}$) ;

6

- ultimate point in tension ($F_{u,t}$, $u_{u,t}$) ;
- displacement ductility capacity in tension ($\mu_t = u_{5\%}/u_{y,t}$);

## 3. Analytical description of the force-displacement response

For the sake of conciseness, the analytical formulations presented in the work are related to the response in tension only of a single CSB device. Further investigations on the response in compression and on the coupled behavior of two CSBs are presented in [22].

The initial elastic behavior of the CSB can be described in terms of the initial lateral stiffness and the first yielding point as evaluated imposing the equilibrium in the undeformed configuration [19,21]:

$$k_{in} = \frac{3}{8} \cdot \frac{E \cdot J \cdot \cos\theta_0}{L_0^3 \cdot \xi_0^2} \tag{3}$$

$$F_{y,t} = \frac{W_e \cdot f_y}{d_0} \cdot \gamma = \frac{f_y \cdot J}{L_0 \cdot h \cdot \xi_0} \cdot \gamma \tag{4}$$

$$u_{y,t} = \frac{8}{3} \cdot \frac{f_y \cdot L_0^2 \cdot \xi_0}{E \cdot h \cdot \cos\theta_0} \cdot \gamma \tag{5}$$

$$\gamma = \frac{1}{1 + \frac{h}{2L_0} \cdot \frac{2}{\xi_0} \cdot \left(\frac{i}{h}\right)^2} \tag{6}$$

$\gamma$ is a reduction factor ($\gamma \leq 1.0$) depending on the simultaneous presence of axial force and bending moment.

The lateral displacement u5% (point P5% corresponding to the configuration $\xi$=5%) results equal to:

$$u_{5\%} = 2L_0 \frac{\left|\left(\cos\theta_{5\%} - \cos\theta_0\right)\right|}{\cos\theta_0} \tag{7}$$

Where $\theta_{5\%}$ indicates the angle $\theta$ corresponding to the configuration with $\xi$=5%.

The displacement us (point Ps corresponding to the achievement of the "straight" configuration of the CSB) can be estimated as the sum of the contributions due to the rigid body rotation (Eq. 1) and due to the elastic deformation $\varepsilon_y$ (just before yielding point due to axial tension):

$$u_s = \frac{2L_0}{\cos\theta_0}\left(1 - \cos\theta_0 + \varepsilon_y\right) \tag{8}$$

The lateral force Fs corresponding to the point Ps can be evaluated according to:

$$F_s = A \cdot f_y \tag{9}$$

Inspection of the analytical equations describing the initial elastic behavior (Eqs. 3-6) reveal that it is governed by the global geometrical parameter $\xi_0$ (related to the initial lever arm $d_0$ and length $L_0$), the material mechanical parameters (E, $f_y$), and the cross-sectional properties (J, $i/h$, $h/L_0$). More in detail, as expected, both the initial stiffness and yielding strength reduce with increasing values of $\xi_0$. In addition, the yielding strength is influenced by the N-M interaction, quantified by parameter $\gamma$, expressed as a function of

7

$\xi_0$, h/2L0 and i/h. It can be noted that $\gamma$ can be interpreted as the reduction factor applied to $\dfrac{W_e \cdot f_y}{d_0}$ that is the yielding strength as evaluated considering the undeformed configuration and the contribution of bending moment only.

Figure 6a displays the trend of $\gamma$ vs $\xi_0$ for selected values of h/2L0 (for i/h=0.29 corresponding to a rectangular cross section). For $\xi_0 > 0.10$, values of $\gamma$ are between 0.8 and 1.0. Moreover, $\gamma$ values tend to decrease with increasing values of *h/2L₀*.

The ratio $u_{5\%}/u_y$ can be considered a measure of the displacement ductility in tension:

$$\mu_t = \frac{3}{4} \frac{E}{f_y} \frac{h}{L_0} \frac{\left|\left(\cos\theta_{5\%} - \cos\theta_0\right)\right|}{\xi_0 \cdot \gamma_{y,t}}$$

(10)

Eq. 10 clearly highlights that the ductility of the CSB depends on the product of three main factors: a factor related to the material mechanical properties (*E/f_y*), a slenderness parameter (*h/2L₀*) and a function

$$f(\xi_0) = \frac{\left|\left(\cos\theta_{5\%} - \cos\theta_0\right)\right|}{\xi_0 \cdot \gamma}$$

dependent on the initial geometrical configuration.

## 4. Direct formulations for preliminary design in the context of PBSD

In the PBSD framework, a performance objective (PO) is defined as the coupling of a building performance level with a given earthquake intensity level [3]. More in detail, each PO can be then identified with a precise request in terms of a structural performance so that mechanical behavior objectives can be identified for the structural system carrying the lateral loads (STEP 2 of the conceptual flowchart of Fig. 2), also referred to as lateral resisting system (LRS). In a previous work, the authors identified the mechanical behavior objectives for the whole LRS in a target initial stiffness ▣, a target first yielding strength ▣, and a target ductility ▣ [19]. From the knowledge of ▣ , ▣ and ▣ for the whole LRS, it is then possible to obtain the corresponding target values ($\overline{k_{in,CSB}}$ , $\overline{F_{y,CSB}}$ and $\overline{\mu_{CSB}}$) for each CSB (STEP 3 of the conceptual flowchart of Fig. 2).

In order to simplify the mathematical expressions and obtain direct analytical equations relating the desired mechanical behavior objectives ($\overline{k_{in,CSB}}$ , $\overline{F_{y,CSB}}$ and $\overline{\mu_{CSB}}$) with the geometrical design parameters of the CSB (STEP 4 of the conceptual flowchart of Fig. 2), it is necessary to introduce the following assumptions:

- $5\% \le \xi_0 \le 25\%$ ;

- first order approximation of the function

$$f(\xi_0) = \frac{\left|\left(\cos\theta_0 - \cos\theta_{5\%}\right)\right|}{\xi_0 \cdot \gamma_{y,t}} \; ;$$

- $\gamma = 1$ ;

- $\cos\theta_0 = 1$ .

From the previous analytical considerations, it is convenient to assume $\xi_0$, h and *J* as geometrical design parameters.

Using the above assumptions, after simple mathematical manipulations of Eq. 3, 4 and 10, the following analytical expressions can be obtained:

8

$$\xi_0 = \frac{0.06 \cdot \rho + \sqrt{0.014 \cdot \rho^2 + 7.8 \cdot \rho \cdot \overline{\overline{\mu_{CSB}}}}}{3.9 \cdot \rho}$$

$$h = \frac{4}{3} \cdot \frac{f_y}{E} \cdot \rho \cdot L_0 \cdot \xi_0$$

$$J = \frac{4}{3} \cdot \frac{\overline{F_{y,CSB}}}{E} \cdot \rho \cdot L_0^{\,2} \cdot \xi_0^{\,2} \tag{11}$$

$$\rho = \frac{2 \cdot \overline{k_{in,CSB}} \cdot L_0}{F_{y,CSB}}$$

where is a non-dimensional parameter.

The actual values of the key mechanical properties of the CSB (namely $\widetilde{k_{in,CSB}}$, $\widetilde{F_{y,CSB}}$ and $\widetilde{\mu_{CSB}}$) are finally determined by means of Eqs. 3, 4 and 10 using the values of *h, J* and $\xi_0$ as computed from Eq. 11. In general the values of $\widetilde{k_{in,CSB}}$, $\widetilde{F_{y,CSB}}$ and $\widetilde{\mu_{CSB}}$ will differ from the corresponding target ones ($\overline{k_{in,CSB}}$, $\overline{F_{y,CSB}}$ and $\overline{\mu_{CSB}}$), since the design equations have been derived based on simplified assumptions.

To evaluate the level of approximation associated with the use of the explicit equations, the graphs of Figure 6 report the trends of the relative errors between the actual values of initial stiffness $\widetilde{k_{in,CSB}}$, yielding force $\widetilde{F_{y,CSB}}$ and ductility $\widetilde{\mu_{CSB}}$ and the corresponding target values $\overline{k_{in,CSB}}$, $\overline{F_{y,CSB}}$, and $\overline{\mu_{CSB}}$, considering $5\% \le \xi_0 \le 25\%$ and values of $h/2L_0$ of 1/50, 2/50 and 4/50. The relative error is computed as (actual value – target value) / actual value and is expressed in %.
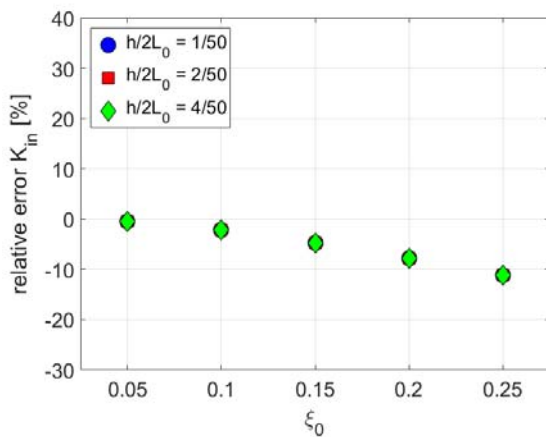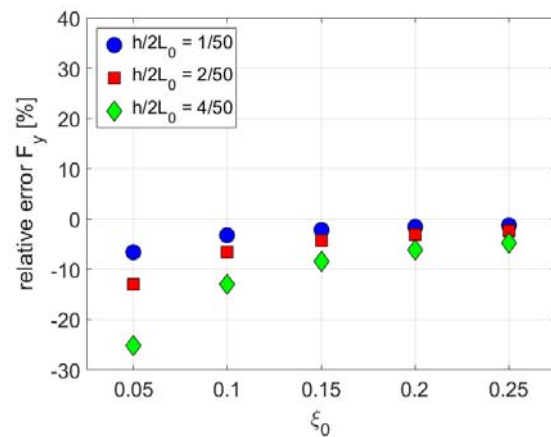


(a)                                              (b)
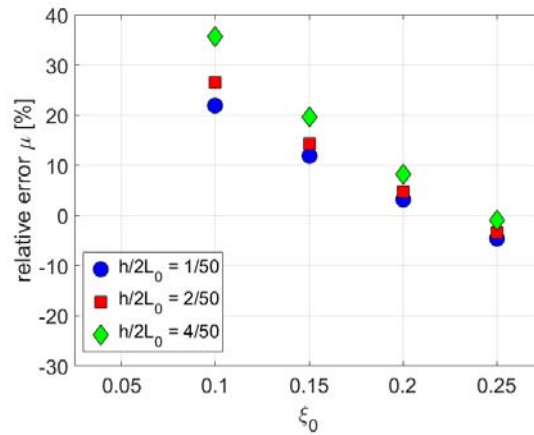
(c)

Figure 6 - Relative errors associated to: (a) initial stiffness; (b) first yielding; (c) ductility.

In general, the relative errors related to the initial stiffness and the yielding force tend to be negative, with values between 0 to -25%. The errors related to the initial stiffness tend to increase (in absolute values) with increasing values of [×], while they are practically independent from $h/2L_0$. In the worst case scenario ([×]=25%) errors are around 10%. The errors associated to the yielding force tend to increase (in absolute values) with increasing values of $h/2L_0$, while they decrease with decreasing values of [×]. In general, they remain under 15%, excluding the worst case of $h/2L_0$ associated with [×]=5%. The relative errors associated to the ductility are in general positive and tend to increase with decreasing values of [×] and with increasing values of $h/2L_0$. In the worst case ([×]=10%), they are between 30- 40%. Note that for [×]=5% the CSB has no ductility.

In case more accurate estimations are required the values of $\xi_0$, $h$ and $J$ given by Eq. 11 can be updated (with few iterations) until the values of $\widetilde{k_{in,CSB}}$, $\widetilde{F_{y,CSB}}$ and $\widetilde{\mu_{CSB}}$ become close enough to the corresponding target ones ($\overline{k_{in,CSB}}$, $\overline{F_{y,CSB}}$, and $\overline{\mu_{CSB}}$).

## Conclusions

The paper investigates the non-linear behaviour of a steel hysteretic brace called Crescent Shaped Brace (CSB), governed by a strong interaction between geometrical and mechanical non-linearity. The attention is devoted to the description of the non-linear behavior through simplified analytical formulations.
First, analytical equations relating the key parameters of the overall force-displacement curve with specific geometrical and mechanical properties of the CSB are obtained. The analytical equations allow to provide insight in the behavior of the CSB.
The following main conclusions can be drawn:
- The initial elastic behavior of CSB (initial stiffness and yielding strength) is governed by the global geometrical parameter $\xi_0$ (normalized initial lever arm), the cross-sectional properties ($J$, $h/2L_0$, $i/h$) and the material properties ($E$, $f_y$), and N-M interaction. In particular, the reduction in the yielding strength due to N-M interaction is quantified by a reduction factor $\gamma$ applied to the first yielding

10

strength as evaluated on the undeformed configuration considering the effect of bending moment only. The reduction becomes small (less than 20%) for values of $\xi_0$ larger than 0.1 and for small values of *h/2L₀*.

- The ductility in tension $\mu_t$ depends on the following parameters: *E/f_y*, *h/2L₀* and a geometrical parameter *f(θ)* related to the initial configuration. It increases with increasing values of $\xi_0$ and *h/2L₀*. An initial lever arm $\xi_0$ larger than 0.1 needs to be adopted to obtain a good ductile behaviour ($\mu_t$ >3.0)

The analytical formulations have also been used to obtain direct design expressions allowing to size the brace in terms of initial lever arm $\xi_0$, cross-sectional moment of inertia *J* and height *h* in order to achieve specific mechanical behavior objectives. It is verified that the direct formulations are sufficiently accurate to be used in the preliminary design phase. They can be also used as first estimations to be improved with few numerical iterations for a more detailed design.

## Acknowledgements

## References

[1]  SEAOC V. Committee (1995) performance-based seismic engineering for buildings. 2000.

[2]  Bozorgnia Y, Bertero VV. Earthquake engineering: from engineering seismology to performance-based engineering. vol. 53. CRC press; 2004. https://doi.org/10.1017/CBO9781107415324.004.

[3]  Bertero RD, Bertero V V. Performance-based seismic engineering: The need for a reliable conceptual comprehensive approach. Earthq Eng Struct Dyn 2002;31:627–52. https://doi.org/10.1002/eqe.146.

[4]  Skinner RI, Kelly JM, Heine AJ. Hysteretic dampers for earthquake-resistant structures. Earthq Eng Struct Dyn 1974;3:287–96.

[5]  Kelly JM, Skinner RI, Heine AJ. Mechanisms of Energy Absorption in Special Devices for Use in Earthquake Resistant Structures. Bull New Zeal Soc Earthq Eng 1972;5:63–73.

[6]  Kato S, Kim YB, Nakazawa S, Ohya T. Simulation of the cyclic behavior of J-shaped steel hysteresis devices and study on the efficiency for reducing earthquake responses of space structures. J Constr Steel Res 2005. https://doi.org/10.1016/j.jcsr.2005.03.006.

[7]  Maleki S, Bagheri S. Pipe damper, Part I: Experimental and analytical study. J Constr Steel Res 2010. https://doi.org/10.1016/j.jcsr.2010.03.010.

[8]  Tyler RG. Tapered Steel Energy Dissipators for Earthquake Resistant Structures. Bull New Zeal Natl Soc Earthq Eng 1978;11:282–94.

[9]  Black CJ, Makris N, Aiken ID. Component testing, seismic evaluation and characterization of buckling-restrained braces. J Struct Eng 2004;130:880–94. https://doi.org/10.1061/(ASCE)0733-9445(2004)130.

[10] Whittaker A, Bertero VV, Alonso J, Thompson C. Earthquake Simulator Testing of Steel Plate Added Damping and Stiffness Elements. 1989. https://doi.org/10.13140/RG.2.1.1455.3207.

[11] Tsai K-C, Chen H-W, Hong C-P, Su Y-F. Design of Steel Triangular Plate Energy Absorbers for Seismic-Resistant Construction. Earthq Spectra 1993;9:505–28. https://doi.org/10.1193/1.1585727.

[12] Li HN, Li G. Experimental study of structure with "dual function" metallic dampers. Eng Struct 2007. https://doi.org/10.1016/j.engstruct.2006.10.007.

11

[13] Chan RWK, Albermani F. Experimental study of steel slit damper for passive energy dissipation. Eng Struct 2008. https://doi.org/10.1016/j.engstruct.2007.07.005.

[14] Garivani S, Aghakouchak AA, Shahbeyk S. Numerical and experimental study of comb-teeth metallic yielding dampers. Int J Steel Struct 2016;16:177–96. https://doi.org/10.1007/s13296-016-3014-z.

[15] Nakashima M, Iwai S, Iwata M, Takeuchi T, Konomi S, Akazawa T, et al. Energy dissipation behaviour of shear panels made of low yield steel. Earthq Eng Struct Dyn 1994;23:1299–313.

[16] Javanmardi A, Ibrahim Z, Ghaedi K, Benisi Ghadim H, Hanif MU. State-of-the-Art Review of Metallic Dampers: Testing, Development and Implementation. Arch Comput Methods Eng 2019. https://doi.org/10.1007/s11831-019-09329-9.

[17] Trombetti T, Silvestri S, Gasparini G, Ricci I. Stiffness-Strength-Ductility-Design Approaches for Crescent Shaped Braces. Open Constr Build Technol J 2009;3:127–40. https://doi.org/10.2174/1874836800903020127.

[18] Palermo M, Ricci I, Gagliardi S, Silvestri S, Trombetti T, Gasparini G. Multi-performance seismic design through an enhanced first-storey isolation system. Eng Struct 2014. https://doi.org/10.1016/j.engstruct.2013.11.002.

[19] Palermo M, Silvestri S, Gasparini G, Trombetti T. Crescent shaped braces for the seismic design of building structures. Mater Struct 2015;48:1485–502. https://doi.org/10.1617/s11527-014-0249-z.

[20] Kammouh O, Silvestri S, Palermo M, Cimellaro GP. Performance-based seismic design of multistory frame structures equipped with crescent-shaped brace. Struct Control Heal Monit 2018;25:1–17. https://doi.org/10.1002/stc.2079.

[21] Palermo M, Pieraccini L, Dib A, Silvestri S, Trombetti T. Experimental tests on Crescent Shaped Braces hysteretic devices. Eng Struct 2017;144:185–200. https://doi.org/10.1016/j.engstruct.2017.04.034.

[22] Palermo M, Laghi V, Gasparini G, Silvestri S, Trombetti T. Analytical formulations for multi-performance seismic design of Crescent Shaped Braces. Eng Struc 2020, *under review*.

12